Supplementary material: Saturation of flames to multiple inputs at one frequency

Håkon T. Nygård[1] †, Giulio Ghirardo[2] and Nicholas A. Worth[1]

[1]Department of Energy and Process Engineering, Norwegian University of Science and Technology, N-7491 Trondheim, Norway

[2]Datadog, 620 8th Ave. 45th floor, New York, NY 10018, USA

Appendix C. Saturation function expression sensitivity analysis

In addition to the saturation function used in this work, as first presented in equation (2.21)

$$F_{\tan}\left(A_q\right) = \frac{2}{1+\sqrt{1+\left(\kappa A_q\right)^2}}\,, \tag{C 1}$$

the three following additional saturation functions are explored

$$F_{\text{step}}\left(A_q\right) = \begin{cases} 1 & \text{for} \quad A_q \leqslant A_{\max} \\ A_{\max}/A_q & \text{for} \quad A_q > A_{\max} \end{cases}\,, \tag{C 2}$$

$$F_{\exp}\left(A_q\right) = e^{-\lambda A_q}\,, \tag{C 3}$$

$$F_{\text{cubic}}\left(A_q\right) = 1 - \gamma A_q^2\,. \tag{C 4}$$

The first additional saturation function, F_{step}, was initially used by Dowling (1997). An exponential expression, $F_{\exp}$, was used in Ghirardo *et al.* (2021). Finally, the cubic heat release rate expression represented by F_{cubic} has been used extensively by Noiray *et al.* (2011). The resulting heat release rate values are shown for a range of acoustic amplitudes A in figure C1 for both spinning ($\chi = \pm\pi/4$) and standing modes ($\chi = 0$). For ease of comparison, the gain and maximum heat release rate amplitude are chosen to be the same for all saturation functions.

The top row of figure C1 shows that the saturation functions in equations (C 1) and (C 2) are monotonically increasing. This is, however, not true for the two remaining functions in the bottom row, given by equations (C 3) and (C 4). The cubic saturation F_{cubic} even results in unphysical negative heat release rate values at sufficiently high amplitudes. As highlighted by Noiray *et al.* (2011), this makes the function only suitable at sufficiently low acoustic amplitudes.

C.1. *Vector field comparisons*

To make a direct qualitative comparison of the fixed point locations and the general features of the vector fields, the nullcline $\left(\widetilde{A}' = 0\right)$ is chosen to have the same amplitude $\widetilde{A}$ for all

† Email address for correspondence: hakon.t.nygard@ntnu.no

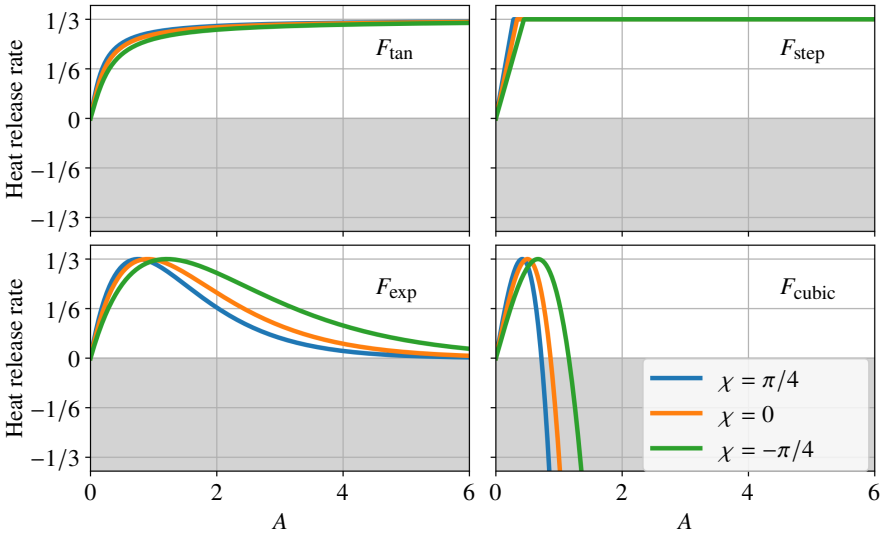

Figure C1: Heat release rate amplitude as a function of acoustic amplitude A using the four different saturation function expressions $F_{\tan}$, F_{step}, $F_{\exp}$, and F_{cubic}. The gain in the linear regime and the maximum heat release rate are chosen to be the same for all saturation functions.

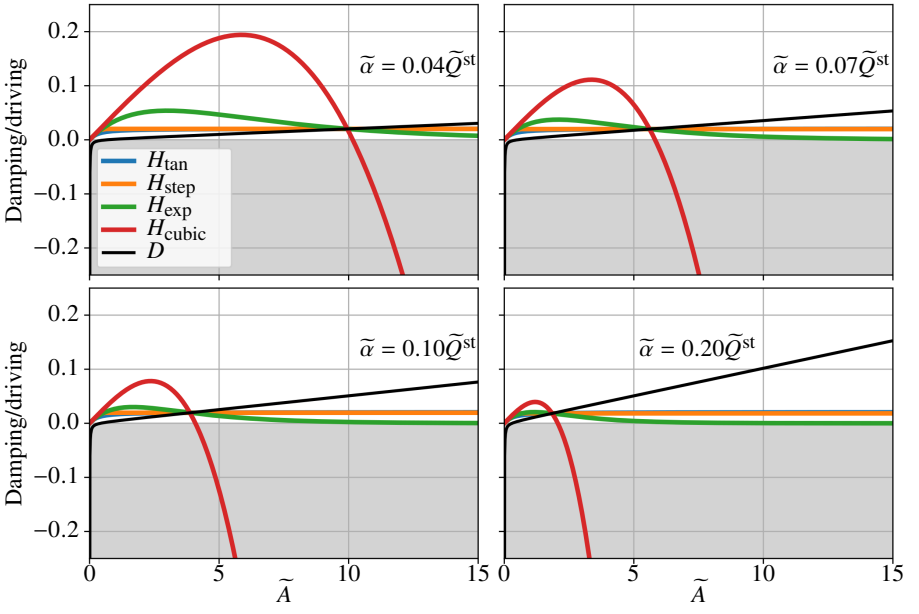

Figure C2: Damping and noise (D) and driving (H) from equation (C 5) for a standing mode ($\chi = 0$). The parameter of each saturation function $F_{\tan}$, F_{step}, $F_{\exp}$, and F_{cubic} is tuned such that the crossing between D and the respective heat release rate term H occur at the same amplitude. This ensures a common amplitude $\widetilde{A}$ when $\widetilde{A}' = 0$ for $\chi = 0$, chosen based on $F_{\tan}$ with $\widetilde{\kappa} = 6$. Each subplot is for a different damping value $\widetilde{\alpha}$.

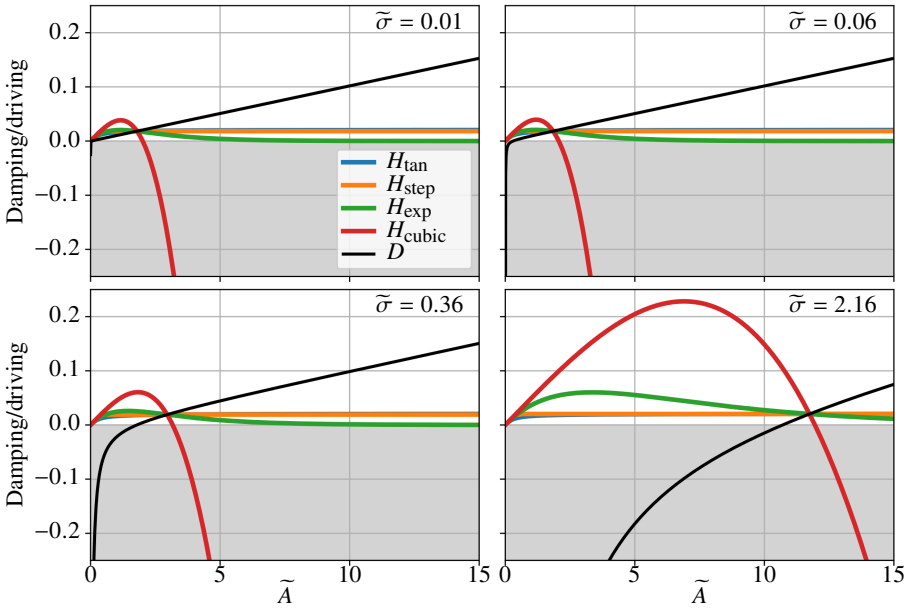

Figure C3: Damping and noise (D) and driving (H) from equation (C 5) for a standing mode ($\chi = 0$). The parameter of each saturation function $F_{\tan}$, F_{step}, $F_{\exp}$, and F_{cubic} is tuned such that the crossing between D and the respective heat release rate term H occur at the same amplitude. This ensures a common amplitude $\widetilde{A}$ when $\widetilde{A}' = 0$ for $\chi = 0$, chosen based on $F_{\tan}$ with $\widetilde{\kappa} = 6$. Each subplot is for a different noise level $\widetilde{\sigma}$.

cases at $\chi = 0$. The governing equation for the amplitude, equation (30a), can be written in non-dimensional form as

$$\widetilde{A}'\left(A, n\theta_0, \varphi, \chi\right) = H\left(\widetilde{A}, n\theta_0, \varphi, \chi\right) - D\left(\widetilde{A}\right), \tag{C 5}$$

where

$$H\left(\widetilde{A}, n\theta_0, \varphi, \chi\right) = \widetilde{A}N^{(0)}\cos\left(\Delta\chi\right) + \frac{1}{2}\widetilde{A}N^{(2n)}\cos\left(2n\theta^{(2n)}\right)\cos\left(2\chi + \Delta\chi\right), \tag{C 6a}$$

$$D\left(\widetilde{A}\right) = \widetilde{\alpha}\widetilde{A} - \frac{\widetilde{\sigma}^2}{4\widetilde{A}}. \tag{C 6b}$$

In the above expressions, the heat release rate source term is given by H, while the acoustic damping α and the deterministic noise term are summarised in D. The two quantities can be plotted as a function of the acoustic amplitude $\widetilde{A}$ for the given nature angle ($\chi = 0$), which is presented in figure C2 and figure C3. Starting with figure C2, the two terms H and D are presented for the different levels of damping explored in figure 5 after tuning the nullcline amplitude at $\chi = 0$ to be the same as for $F_{\tan}$ with $\widetilde{\kappa} = 6$. While the maximum heat release rate is relatively constant for the saturation F_{step}, it is observed to vary significantly for the two remaining saturation schemes. Similar observations are made in figure C3 as the noise level increases. More importantly, without the tuning of the nullcline amplitude at standing modes, the heat release rate at the highest noise level would become a strong damper.

The resulting vector fields for the effect of damping and the effect of noise level, which are equivalent to figures 5 and 9 respectively, are shown in figures C4 and C5. While there are some quantitative differences between the plots, the main qualitative features are very

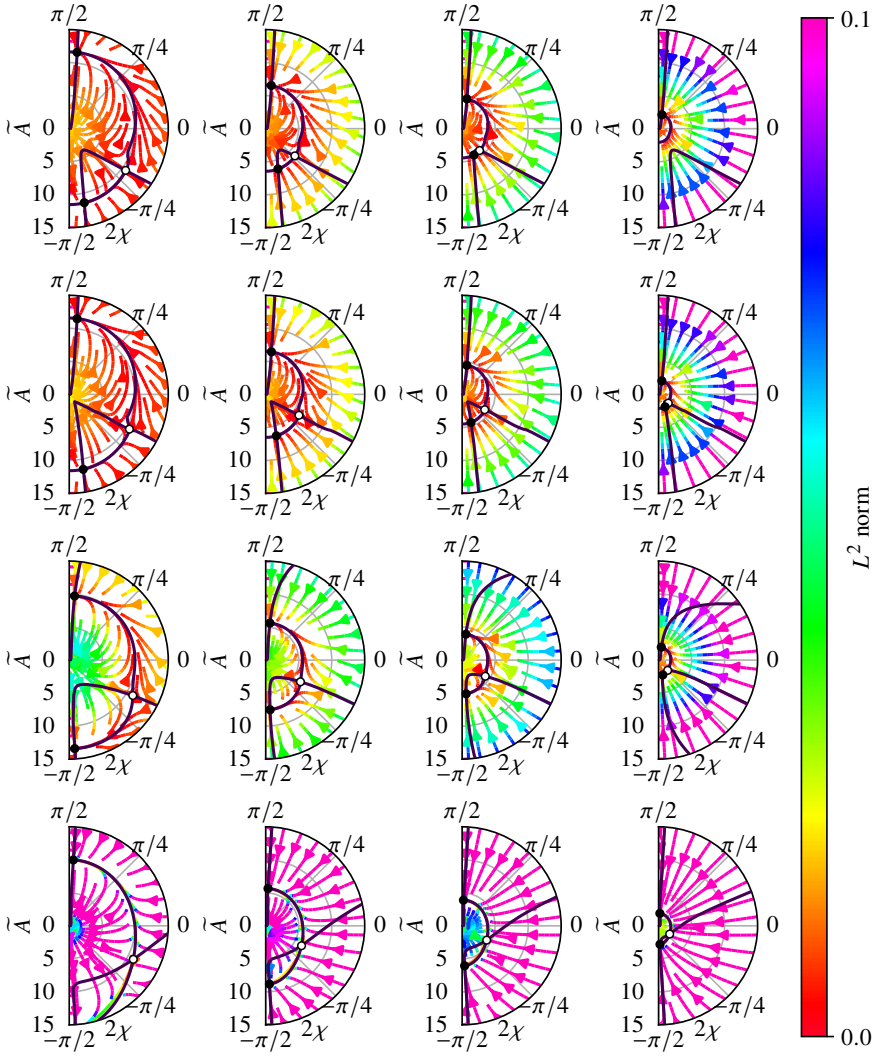

Figure C4: Vector fields for different damping levels (columns) using four different saturation functions (rows) assuming a common preferred heat release rate value for a standing mode ($\chi = 0$). From top to bottom, the saturation functions used are $F_{\tan}$, F_{step}, $F_{\exp}$, and F_{cubic}. The damping values from left to right column are $\widetilde{\alpha} = 0.04\widetilde{Q}^{\text{st}}$, $\widetilde{\alpha} = 0.07\widetilde{Q}^{\text{st}}$, $\widetilde{\alpha} = 0.10\widetilde{Q}^{\text{st}}$, and $\widetilde{\alpha} = 0.20\widetilde{Q}^{\text{st}}$. The top row is the same as figure 5 in the manuscript.

similar. Starting with the damping effect in figure C4, all cases are observed to have a similar connected χ' nullcline in the southern hemisphere, and a separate line in the northern hemisphere. While there are slight differences in when the saddle node bifurcation occurs, it is present for all the different saturation functions.

Similarly, for the increasing noise levels in figure C5, the same features are observed for all the saturation function choices. As the noise increase, the two most southern solutions

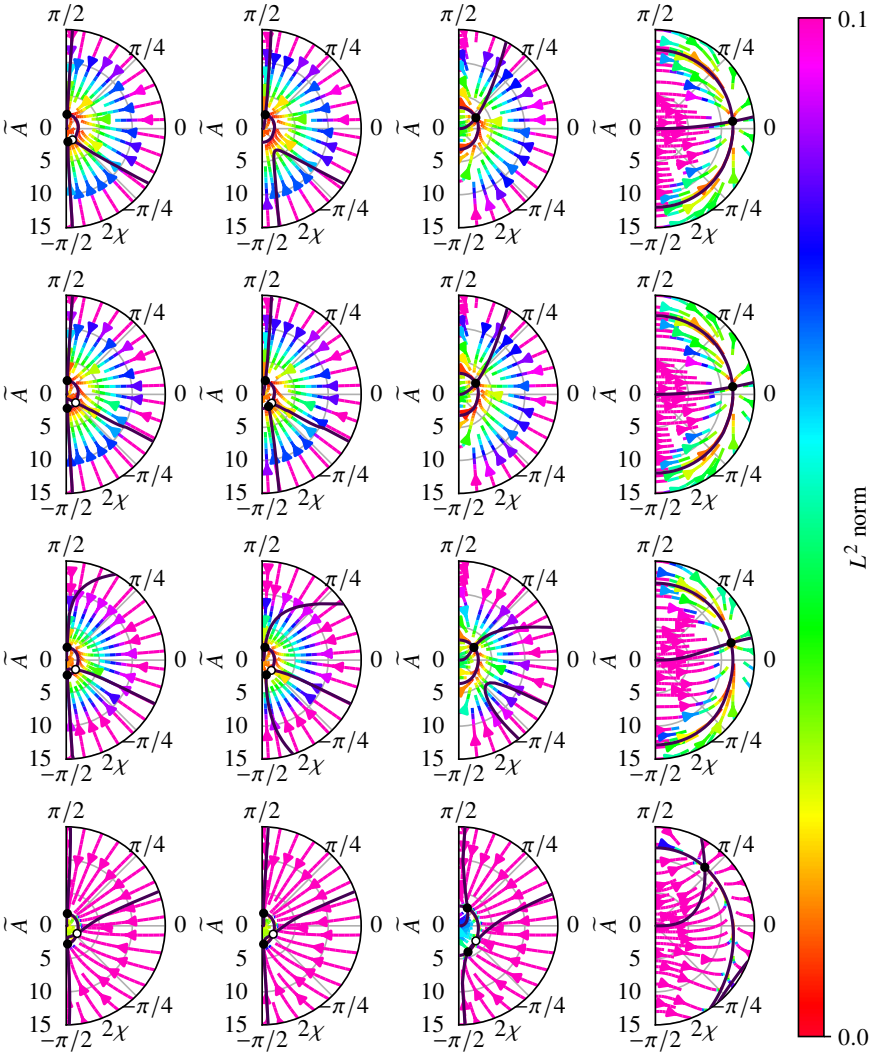

Figure C5: Vector fields at different noise levels (columns) for four different saturation functions (rows) assuming a common preferred heat release rate value for a standing mode ($\chi = 0$). From top to bottom, the saturation functions used are $F_{\tan}$, F_{step}, $F_{\exp}$, and F_{cubic}. The noise levels from left to right column are $\widetilde{\sigma} = 0.01$, $\widetilde{\sigma} = 0.06$, $\widetilde{\sigma} = 0.36$, and $\widetilde{\sigma} = 2.16$. The top row is the same as figure 9 in the manuscript.

disappear, albeit at slightly different parameter combinations again. In all the cases, the initially ACW spinning fixed point also moves closer to a standing mode solution as the noise increase. In summary, all the saturation functions have the same qualitative behaviour with some quantitative differences for a given parameter combination.

Finally, it should again be noted that to achieve the results in this section, the parameter of each saturation function in equations (C 2) to (C 4) was adjusted for each column to have the same acoustic amplitude as equation (C 1) with $\widetilde{\kappa} = 6$ at $A'|_{\chi=0} = 0$. Keeping the

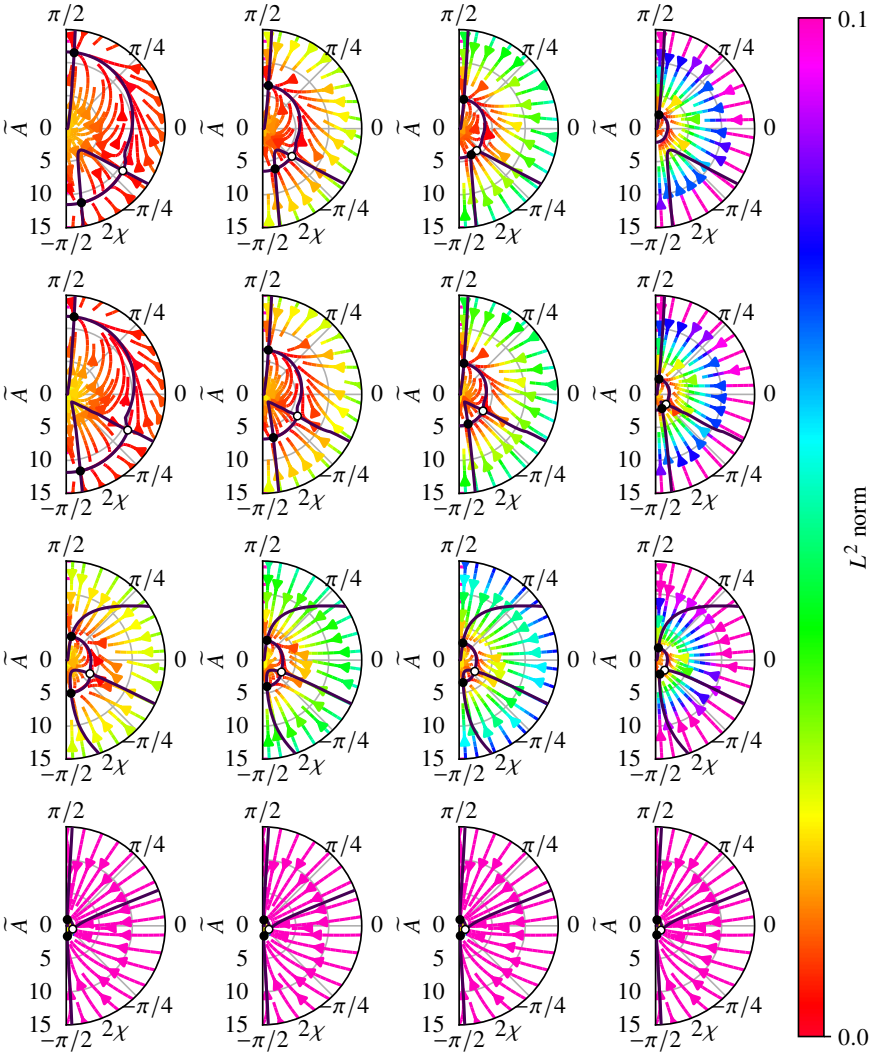

Figure C6: Vector fields for different damping levels (columns) using four different saturation functions (rows) assuming a common maximum heat release rate value. From top to bottom, the saturation functions used are $F_{\tan}$, F_{step}, $F_{\exp}$, and F_{cubic}. The damping values from left to right column are $\widetilde{\alpha} = 0.04\widetilde{Q}^{\text{st}}$, $\widetilde{\alpha} = 0.07\widetilde{Q}^{\text{st}}$, $\widetilde{\alpha} = 0.10\widetilde{Q}^{\text{st}}$, and $\widetilde{\alpha} = 0.20\widetilde{Q}^{\text{st}}$. The top row is the same as figure 5 in the manuscript.

saturation function parameters constant for the different system parameter combinations is briefly presented in the next section.

C.2. *Same maximum heat release rate*

In this section, the parameter of each saturation function is chosen such that the maximum heat release rate is common to all the saturation functions, as displayed in figure C1. The effect of damping explored in figure C4 is presented for a constant saturation function parameter

in figure C6. Again, the two top rows, using equations (C 1) and (C 2), show very similar results to each other. This could already be predicted directly from figure C2, where both functions provide similar valued H functions for the explored range of damping levels. The amplitude of the $A' = 0$ nullcline is, however, lower for the other functions due to how the heat release rate amplitude starts dropping for sufficiently high amplitudes. This could either be addressed by adjusting the saturation function parameters, as in the previous section, or possibly by adjusting the system parameters to more suitable values for the given saturation function parameters.

Similarly, figure C7 show that $F_{\tan}$ and F_{step} yield qualitatively the same results due to how close the resulting H values are. In this case, the exponential saturation $F_{\exp}$ also have a very similar behaviour, but the cubic heat release rate expression in the bottom row yields very different results. When the noise level is sufficiently high, the heat release rate amplitude is in fact negative, as highlighted when discussing figure C3. In this case the heat release rate is acting as an acoustic damper instead of a source term, which is unphysical.

REFERENCES

Dowling, A. P. 1997 Nonlinear self-excited oscillations of a ducted flame. *Journal of Fluid Mechanics* **346**, 271–290.

Ghirardo, G., Nygård, H. T., Cuquel, A. & Worth, N. A. 2021 Symmetry breaking modelling for azimuthal combustion dynamics. *Proceedings of the Combustion Institute* **38** (4), 5953–5962.

Noiray, N., Bothien, M. & Schuermans, B. 2011 Investigation of azimuthal staging concepts in annular gas turbines. *Combustion Theory and Modelling* **15** (5), 585–606.

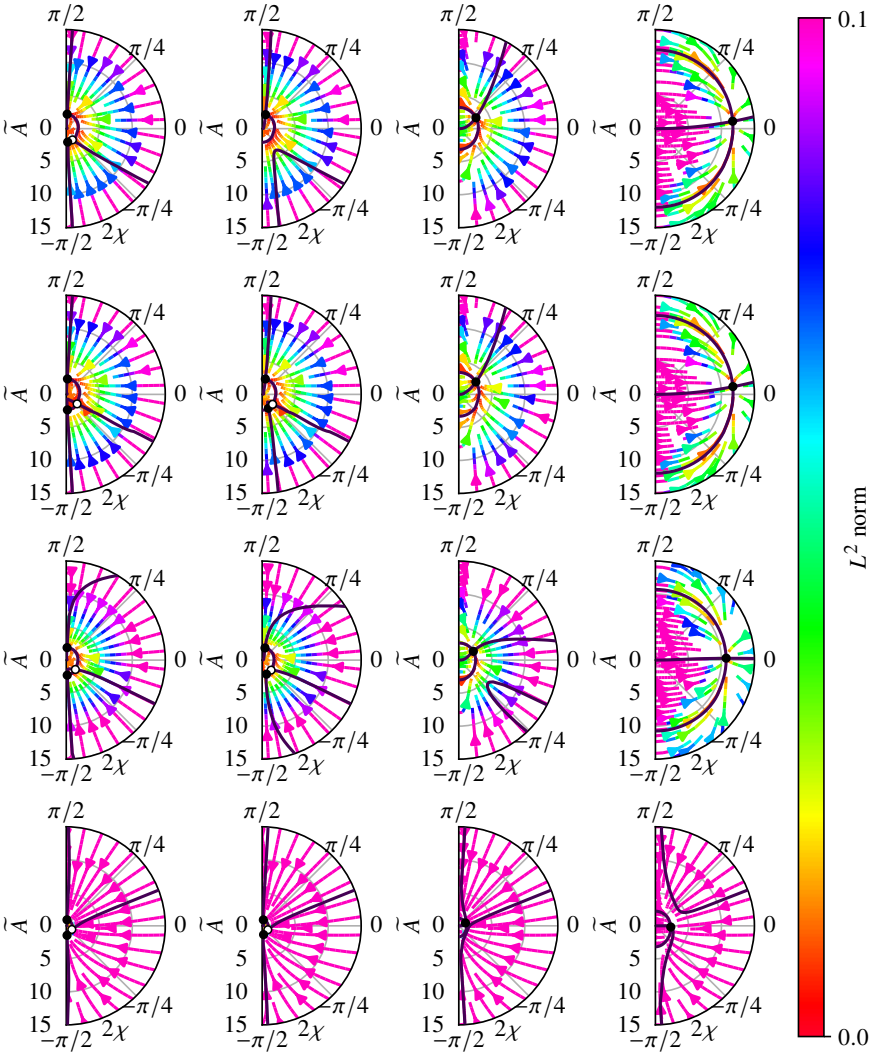

Figure C7: Vector fields at different noise levels (columns) for four different saturation functions (rows) assuming a common maximum heat release rate value. From top to bottom, the saturation functions used are $F_{\tan}$, F_{step}, $F_{\exp}$, and F_{cubic}. The noise levels from left to right column are $\widetilde{\sigma} = 0.01$, $\widetilde{\sigma} = 0.06$, $\widetilde{\sigma} = 0.36$, and $\widetilde{\sigma} = 2.16$. The top row is the same as figure 9 in the manuscript.